Transmittance of subwavelength optical tunnel junctions

Christian Girard
CEMES, UPR CNRS 8011, 29 rue Jeanne Marvig, Boîte Postale 4347, F-31055 Toulouse Cedex 4, France
(Received 6 April 1998; revised manuscript received 4 June 1998)

Photonic transfer through constrictions with subwavelength lateral size is at the origin of important near-field optics developments. In this paper, we adapt the integral representation of Maxwell's equations to implement a realistic three-dimensional model of subwavelength optical constriction (SOC). We apply this scheme to investigate the optical properties of different SOC geometries. In particular, from the energy flow exiting the SOC we analyze the transmittance capability of such systems as a function of different external parameters. Preliminary steps toward the implementation of three-dimensional simulators of near-field microscopes are discussed. [S0163-1829(98)04439-7]

According to the Rayleigh criterion, an elongated optical constriction cannot transmit visible light over a micrometer distance if its cross section becomes smaller than the incident wavelength λ. For a section of dimension much smaller than λ, the collected electromagnetic energy will decay exponentially with the constriction length. In spite of this fundamental limitation, several situations of photonic transport through subwavelength optical constrictions (SOC) have be identified. The first one concerns mainly scanning near-field optical microscopy (SNOM),[1] in which subwavelength-sized patterns lying on a surface are optically imaged by approaching a pointed fiber close enough to the object to detect the evanescent waves. In these experiments, the reduction of the tip-sample spacing below the tunneling decay length makes the energy transfer possible. The second observation of such peculiar effects is more recent,[2] and concerns a similar phenomenon in which the optical transmittance of subwavelength holes arrays fabricated inside metallic films presents dramatic enhancements.

All these experiments raised several important questions concerning the physical mechanisms underlying photonic transport in mesoscopic and nanometric optical systems. Among all these numerous questions, both numerical evaluation and optimization of the transferred energy rate were not completely assessed. For example, until now the calculation of the transmittance coefficient of an optical constriction with respect to the different internal and external parameters (tip composition, external illumination mode, incident wavelength, gap length, etc.) have been rather scarce.

Very recently, an original approach to this problem has been detailed in a work by Ward and Pendry.[3] In their paper, these authors employed a *transfer-matrix method* currently applied in the theory of photonic band gap. By using an adaptative coordinate transformation they were able to model realistic SNOM tip designs and to realize a comparative analysis of transmission efficiencies.

In the present paper, we discuss an alternative method for solving this challenging problem. It is based on a peculiar adaptation of the integral representation of Maxwell's equations. We apply this scheme to investigate the optical properties of different SOC architectures. In particular, from the energy flow exiting the SOC, we analyze the transmittance capability of such systems as a function of different external parameters. Several specific geometries will be discussed and compared with experimental measurements.

As a starting point, let us consider the simple planar optical junction formed by three dielectric media of optical indexes n_1, n_2, and n_3 (with $n_1 > n_2$). When such a junction is illuminated in total internal reflection in the first medium n_1, its transmittance T (defined by the normalized energy flux transmitted in the third medium) displays a quasiexponential decay with respect to the spacing L_0.[4] Beyond the contact region between the two plates we can approximate this coefficient by the well-known exponential law

$$T(L_0) = A \exp[-\Gamma(\theta_0, k_0) L_0], \tag{1}$$

where the decay factor $\Gamma = 2[n_1^2 \sin(\theta_0)^2 - n_2^2] k_0$ depends only on the incident angle θ_0 and the wave vector modulus k_0 in vacuum. The factor A depends on the polarization mode used to illuminate the system.

Now let us see what happens when a three-dimensional (3D) microtip supported by the *output* medium is inserted in the gap (cf. insets in Fig. 1). In this case, the initial electric and magnetic fields $\mathbf{E_0}(\mathbf{r},\omega)$ and $\mathbf{B_0}(\mathbf{r},\omega)$ generated inside the planar junction are strongly modified by the microtip. As demonstrated in Refs. 5 and 6, the new electromagnetic field state $\{\mathcal{E}(\mathbf{r},\omega), \mathcal{B}(\mathbf{r},\omega)\}$ can be derived everywhere in the junction by introducing two generalized propagators labeled $\mathcal{K}(\mathbf{r},\mathbf{r}',\omega)$ and $\mathcal{L}(\mathbf{r},\mathbf{r}',\omega)$, respectively:

$$\mathcal{E}(\mathbf{r},\omega) = \int_v \mathcal{K}(\mathbf{r},\mathbf{r}',\omega) \cdot \mathbf{E}_0(\mathbf{r}',\omega) d\mathbf{r}' \tag{2}$$

and

$$\mathcal{B}(\mathbf{r},\omega) = \int_v \mathcal{L}(\mathbf{r},\mathbf{r}',\omega) \cdot \mathbf{E}_0(\mathbf{r}',\omega) d\mathbf{r}', \tag{3}$$

where the integral runs over the volume occupied by the microtip. As detailed in Refs. 5 and 6, the dyadic $\mathcal{K}(\mathbf{r},\mathbf{r}',\omega)$, also called *generalized electric-field propagator*, can be formulated in terms of the optical field susceptibility tensor $\mathcal{S}(\mathbf{r},\mathbf{r}',\omega)$ associated with the entire system:

$$\mathcal{K}(\mathbf{r},\mathbf{r}',\omega) = \delta(\mathbf{r}-\mathbf{r}') + \mathcal{S}(\mathbf{r},\mathbf{r}',\omega) \cdot \chi_{tip}(\mathbf{r}',\omega), \tag{4}$$

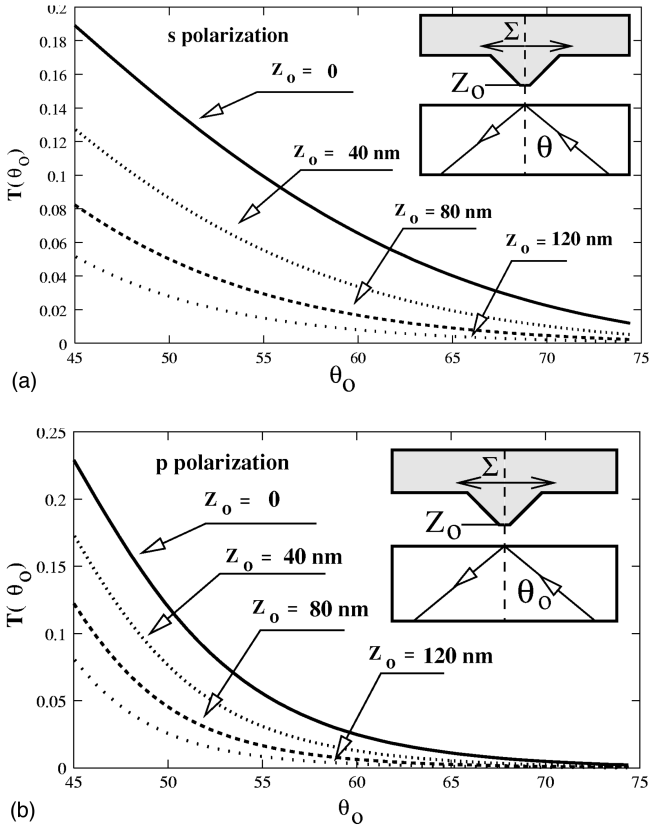

FIG. 1. Angular variation of the STOM/PSTM transmittance for different tip-sample distances: (a) Calculation performed in the *s*-polarized mode. (b) Same calculation, but in the *p*-polarized mode.

where $\chi_{tip}(\mathbf{r}',\omega)$ represents the linear electric susceptibility of the microtip. The second propagator $\mathcal{L}(\mathbf{r},\mathbf{r}',\omega)$ establishes a direct relation between incident electric field and local magnetic field. When dealing with nonmagnetic materials, it may be expressed as a functional of $\mathcal{K}(\mathbf{r},\mathbf{r}',\omega)$:

$$\mathcal{L}(\mathbf{r},\mathbf{r}',\omega)=\frac{\delta(\mathbf{r}-\mathbf{r}')}{ik_0}\Lambda_{\mathbf{r}'} + \int_v \mathbf{Q}_0(\mathbf{r},\mathbf{r}',\omega)\cdot\chi_{tip}(\mathbf{r}'',\omega)\mathcal{K}(\mathbf{r}'',\mathbf{r}',\omega)d\mathbf{r}'', \tag{5}$$

where $\Lambda_{\mathbf{r}'}$ labels the matrix form of the *curl* operator and $\mathbf{Q}_0(\mathbf{r},\mathbf{r}',\omega)$ represents the so-called *electric-magnetic mixed susceptibility* of the bare junction. Analytical forms of all these tensors can be easily derived from our previous works.[6,7]

In that scheme, the field-susceptibility tensor $\mathcal{S}$ required to obtain the *generalized field propagator* $\mathcal{K}(\mathbf{r},\mathbf{r}',\omega)$, can be derived from the appropriate discretized form of Dyson's equation over the whole volume occupied by the tip:

$$\mathcal{S}(\mathbf{r}_i,\mathbf{r}_j,\omega)=\mathbf{S_0}(\mathbf{r}_i,\mathbf{r}_j,\omega) + \sum_{k=1}^{n}\chi_{tip}(\mathbf{r}_k,\omega)\cdot\mathbf{S_0}(\mathbf{r}_i,\mathbf{r}_k,\omega)\cdot\mathcal{S}(\mathbf{r}_k,\mathbf{r}_j,\omega), \tag{6}$$

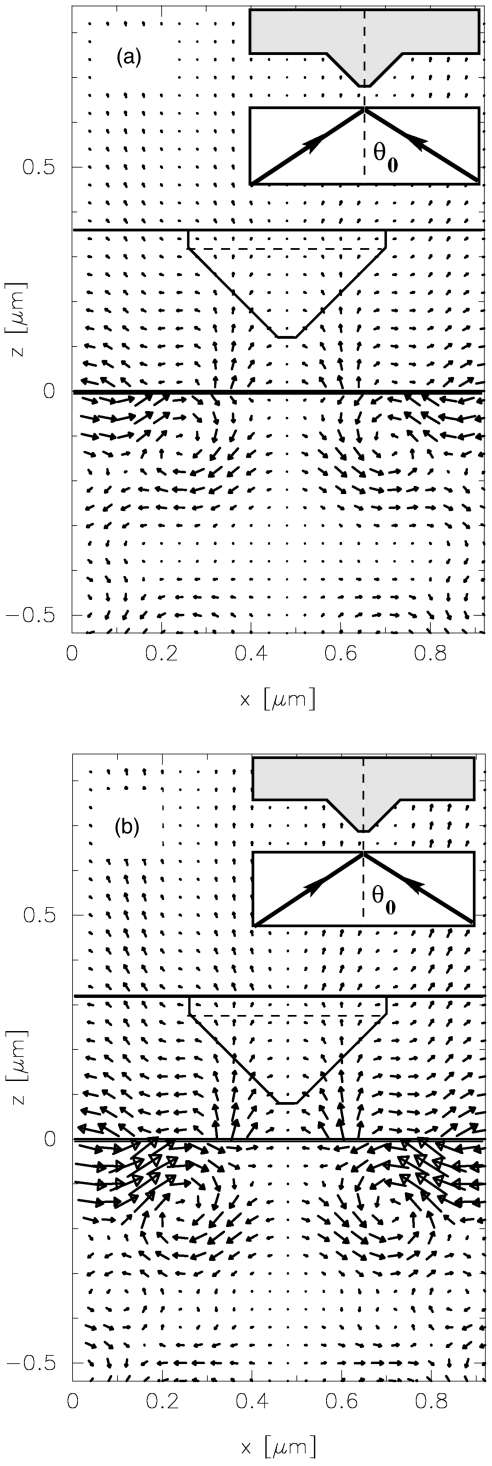

FIG. 2. Planar projection of the time-averaged Poynting $\mathcal{P}(x,y=cst,z)$ vector in a (XOZ) plane cutting the microtip center. As described by the inset, the SOC is illuminated by two counterpropagating surfaces waves. (a) $Z_0=80$ nm. (b) $Z_0=40$ nm.

where the entire tip volume has been divided into n meshes of volume τ_i centered at $\mathbf{r_i}$, $(\mathbf{i}=1,\ldots,n)$. After solving Eq. (6), and backsubstitution of the resulting matrix into Eq. (4) we get the *generalized field propagator* $\mathcal{K}$ inside the source region (the 3D microtip) for a given incident wavelength $\lambda=2\pi/\omega$. In a second step, the informations generated by this numerical run can be used to propagate, via Eqs. (2) and (3),

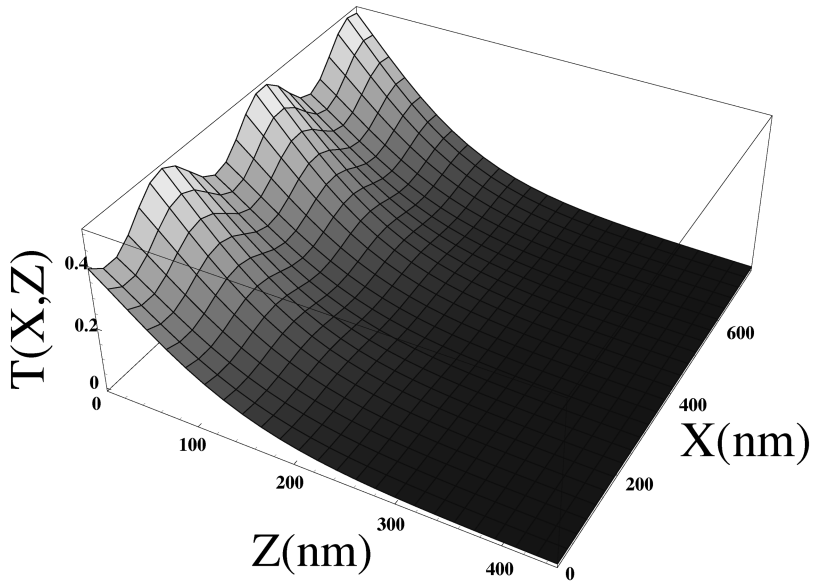

FIG. 3. Numerical simulation of the spatial modulation of the standing evanescent wave along the propagation direction of two interfering waves (*OX* axis) and the exponential decay occurring when increasing the tip-sample distance Z_0.

the electromagnetic field $\{\mathcal{E}(\mathbf{r},\omega),\mathcal{B}(\mathbf{r},\omega)\}$ everywhere in the system. The time-average Poynting vector field is then defined by

$$\mathcal{P}(\mathbf{r}) = \tfrac{1}{2}\mathrm{Re}\{\mathcal{E}(\mathbf{r},\omega)\wedge\mathcal{B}^*(\mathbf{r},\omega)\}. \tag{7}$$

Finally, from the information contained in Eq. (7), we are able to define a transmission coefficient characterizing the optical transparence of the SOC. This quantity will be normalized with respect to the incident energy E_{inc} crossing a surface Σ located inside the input medium and centered around the microtip (cf. Fig. 2):

$$T(Z_0,\theta_0,\lambda) = \frac{\int_\Sigma \mathcal{P}(\mathbf{l},Z_0+Z_\Sigma)\cdot\mathbf{u_z}d\mathbf{l}}{E_{inc}}, \tag{8}$$

where Z_Σ defined the location of the surface Σ in the *output* medium of the SOC, $\mathbf{l}=(x,y)$, and $\mathbf{u_z}$ is a unit vector directed along the *OZ* axis.

The numerical method described above is now sufficiently mature to faithfully reproduce different experimental processes at work in real experiments (imaging, local spectroscopy, optical binding forces, etc.). In the following, we focus our applications on two specific configurations related to *subwavelength optics*.

Among the numerous SNOM configurations, the so-called *tunneling configuration* (STOM/PSTM) (Refs. 8–16) occupies a singular place in the NFO community because of its intriguing analogies with the scanning tunneling microscope.[17] In this microscope, a significant amount of the energy associated with the evanescent surface wave is coupled with a microtip that is raster scanned across the sample to be imaged. In this context, the most direct application of our model concerns the reproduction of the detected intensity curves $I(Z_0,\theta_0)$ (Refs. 18 and 19) that can be obtained when varying both external polarization and illumination conditions. This energy is proportional to the transmission coefficient $T(Z_0,\theta_0,\lambda)$ of the junction, and depends on the incident illumination energy. The tip chosen to calculate $T(Z_0,\theta_0,\lambda)$, is a tetraedrally shaped protrusion where four faces and four sharp edges converge in a common tip ending with a small curvature radius ($r_{tip}=40$ nm).

In the applications described in Fig. 1, the following physical parameters have been used: (a) tip height $H=240$ nm, (b) tip aperture angle $\alpha=90°$, (c) optical index $n_1=n_3=n_{tip}=1.5$, (d) integration area $\Sigma=1\ \mu\mathrm{m}^2$, and (e) incident wavelength $\lambda=600$ nm. From these parameters we have addressed the question of the decay of the normalized intensity as a function of the incident angle (cf. Fig. 1). Some comments can be made about these results. (i) As expected, the model reproduces correctly the decay of the SOC transmittance when increasing the incident angle or the tip-sample distance. (ii) According to experimental measurements,[19] both *s*- and *p*-polarized modes behave differently. For a moderate angle range ($45°<\theta_0<53°$), the signal intensity detected in the *p* mode dominates the intensity that can be measured by switching the system on the *s* mode. Beyond this angular value, we observe, in fairly good agreement with experimental data,[19] a second regime in which the *s* mode becomes progressively more efficient than the *p* mode when approaching the grazing angle. (iii) Finally, we have checked that by increasing the tip size (radius and height), the well-known deviation to the exponential law in the region where the optical contact occurs is well recovered.[8,18,19]

Our second application deals with the interference of two evanescent surface waves. The observation of this intriguing optical phenomena was first reported by Meixner, Bopp, and Tarrach in the STOM/PSTM configuration.[20] This illumination mode may be achieved in a very simple way in the STOM/PSTM configuration by using a glass prism with a metallized side. In the absence of a pointed detector, a simple calculation indicates that the resulting incident field does not propagate in the OZ direction nor in the (XOY) plane. In this case, along the surface of the sample, the electric field verifies the equation

$$\mathbf{E_0}(\mathbf{r},\omega) = 2\mathbf{E_0}e^{-\Gamma z}e^{-i\,\omega t}\cos(\mathbf{k}\cdot\mathbf{l}), \tag{9}$$

where the parameter Γ is identical to the decay length occurring in Eq. (1), and $\mathbf{k}=k_0\sin(\theta_0)\mathbf{u_x}$. According to usual symmetry principles, it is easy to intuitively predict that no Poynting vector field can exist in the absence of detection process ($Z_0\rightarrow\infty$). Consequently, such particular conditions prevent all photonic energy transfer in the junction. This equilibrium state will only be interrupted when the tip enters the stationary evanescent wave. In this case, the localized interaction will open an efficient radiative channel along the *OZ* direction. A meaningful illustration of this phenomena is provided in Fig. 2, where we observed the creation of an energy flux exiting the junction. As expected and confirmed by Fig. 2(b) decreasing the tip-sample gap tends to reinforce the energy flux strongly toward the *output* medium. In this simulated example, the tip is located above an initially dark fringe, so that the conversion process originates essentially from the near-field coupling between the tip faces and the tails of two adjacent bright fringes. Finally, we can observe two quasicircular electromagnetic vortices in the region of the *input medium* located near the tip. This quasistationary regime is induced by the symmetrical interaction of the two countrapropagating beams with the lateral faces of the SOC. We have also reproduced numerically the 3D map of the standing evanescent wave (cf. Fig. 3 of Ref. 20). In this last application (cf. Fig. (3); the tip is raster scanned along the *OX* axis by increasing the tip-sample distance after each scanline. Such a representation allows the decay as well as the modulation of the standing surface wave to be represented simultaneously. From this map it is easy to extract the ratio η between the amplitude of the modulation and the average detected intensity. In fact this parameter provides us with information on the finite effective diameter of the tip. In good agreement with experimental data gathered in Ref. 20, the ratio η calculated from the parameters listed above does not exceed 0.3 in the near zone.

In conclusion, we believe that the real-space methology summarized in this paper should rapidly give rise to a class of local probe simulators that could assist the experimentalist during acquisition data stage. In the near future, our main objective is the implementation of a numerical STOM/PSTM with spectropic and imaging capabilities of miscellaneous samples. Preliminary benchmarks performed on mesoscopic parallel computers indicate an excellent performance of our code when increasing the number of processors. This parallelization facility is inherent to the self-consistent procedure that proceeds iteratively inside the source region (i.e., the pointed tip in our applications).

The author has benefited from useful discussions with A. Dereux, J. C. Weeber, O. J. F. Martin, and J. P. Goudonnet during the preparation of this paper.

[1] *Near Field Optics*, Vol. 242 of *NATO Advanced Study Institute*, Series E: Applied Sciences, edited by D. W. Pohl and D. Courjon (Kluwer, Dordrecht, 1993), and references therein; M. A. Paesler and P. J. Moyer, *Near-Field Optics: Theory, Instrumentation, and Applications* (Wiley-Interscience, New York, 1996).

[2] T. W. Ebbesen, H. J. Lezec, H. F. Ghaemi, T. Thio, and P. A. Wolff, Nature (London) **391**, 667 (1998).

[3] A. J. Ward and J. B. Pendry, J. Mod. Opt. **44**, 1703 (1997).

[4] M. Born and E. Wolf, *Principles of Optics*, 6th ed. (Pergamon, Oxford, 1980).

[5] O. J. F. Martin, C. Girard, and A. Dereux, Phys. Rev. Lett. **74**, 526 (1995).

[6] Ch. Girard, J. C. Weeber, A. Dereux, O. J. F. Martin, and J. P. Goudonnet, Phys. Rev. B **55**, 16 487 (1997), and references therein.

[7] Ch. Girard, O. J. F. Martin, and A. Dereux, Phys. Rev. Lett. **75**, 3098 (1995).

[8] R. C. Reddick, R. J. Warmack, and T. L. Ferrell, Phys. Rev. B **39**, 767 (1989).

[9] D. Courjon, K. Sarayeddine, and M. Spajer, Opt. Commun. **71**, 23 (1989).

[10] J. Cites, M. F. M. Sanghadasa, C. C. Sung, R. C. Reddick, R. J. Warmack, and T. L. Ferrell, J. Appl. Phys. **71**, 7 (1992).

[11] R. C. Reddick, R. J. Warmack, D. W. Chilcott, S. L. Sharp, and T. L. Ferrell, Rev. Sci. Instrum. **61**, 3669 (1990).

[12] T. L. Ferrell, S. L. Sharp, and R. J. Warmack, Ultramicroscopy **42–44**, 408 (1992).

[13] D. Courjon, C. Bainier, and M. Spajer, J. Vac. Sci. Technol. B **10**, 2436 (1992).

[14] F. de Fornel, L. Salomon, P. Adam, E. Bourillot, J. P. Goudonnet, and M. Nevière, Ultramicroscopy **42–44**, 422 (1992).

[15] N. F. van Hulst, F. B. Segerink, F. Achten, and B. B. Bölger, Ultramicroscopy **42–44**, 416 (1992).

[16] N. F. van Hulst, M. H. Moers, and B. Bölger, J. Microsc. **171**, 95 (1993).

[17] G. Binnig and H. Rohrer, Helv. Phys. Acta **55**, 726 (1982).

[18] J. M. Vigoureux, Ch. Girard, and D. Courjon, Opt. Lett. **14**, 1039 (1989).

[19] L. Salomon, F. de Fornel, and J. P. Goudonnet, J. Opt. Soc. Am. A **8**, 2009 (1991).

[20] A. Meixner, M. Bopp, and G. Tarrach, Appl. Opt. **33**, 7995 (1994).